Surv Geophys (2009) 30:355–376
DOI 10.1007/s10712-009-9073-3

ORIGINAL PAPER

Array Triplication Data Constraining Seismic Structure and Composition in the Mantle

Yi Wang · Lianxing Wen · Donald Weidner

Received: 15 October 2008 / Accepted: 22 May 2009 / Published online: 18 June 2009

Abstract Seismic data recorded in the upper mantle triplication distance range between 10° and 30° are generated by wave propagation through complex upper mantle structure. They can be used to place constraints on seismic velocity structures in the upper mantle, key seismic features near the major discontinuities, and anisotropic structure varying with depth. In this paper, we review wave propagation of the upper mantle triplicated phases, how different key seismic features can be studied using upper mantle triplicated data, and the importance of those seismic features to the understanding of mantle temperature and composition. We present two examples of using array triplicated phases to constrain upper mantle velocity structures and detailed features of a certain discontinuity, with one for a shallow event and the other for deep events. For the shallow event, we present examples of how the array triplication data can be used to constrain several key properties of the upper mantle: existence of a lithospheric lid, existence of a low velocity zone beneath the lithospheric lid, and P/S velocity ratio as a function of depth. For deep events, we show examples of how array triplication data can be used to constrain the detailed structures of a certain discontinuity: velocity gradients above and below the discontinuity, velocity jumps across the discontinuity and depth extents of different velocity gradients. We discuss challenges of the upper mantle triplication study, its connection to other approaches, and its potential for further studying some other important features of the mantle: the existence of double 660-km discontinuities, existence of low-velocity channels near major discontinuities and anisotropy varying with depth.

Keywords Triplication data · Upper mantle · Velocity structures · Upper mantle discontinuity · Mantle composition

Y. Wang (✉) · L. Wen · D. Weidner
Department of Geosciences, State University of New York at Stony Brook, Stony Brook, NY 11794, USA
e-mail: yiwang1@ic.sunysb.edu

L. Wen
e-mail: Lianxing.Wen@sunysb.edu

D. Weidner
e-mail: dweidner@notes.cc.sunysb.edu

1 Introduction

At the epicentral distance range of 10°–30°, seismic waves turn at various depths of the Earth's mantle. Because of the velocity jumps at various upper mantle discontinuities in the mantle, several branches of seismic wave exist, including the waves turning above and below the discontinuities and the reflection from the discontinuities. This distance range is called the triplication distance range.

Because the triplicated waves turn at various depths, seismic studies using upper mantle triplication data played an important role in inferring seismic profiles with depth and in identifying many unique seismic features in the mantle. Because of the limited coverage of triplication data, most previous triplication studies focus on North America, southern Africa, eastern Asia and the Fiji-Tonga region, where triplication data are available. In the Canadian Shield, southern Africa, triplication data are used to constrain the upper mantle velocity structure beneath cratons: the presence and thickness of a lithospheric lid, and the presence and velocity reduction of a low velocity zone (Grand and Helmberger 1984a; LeFevre and Helmberger 1989; Zhao et al. 1999; Simon et al. 2002; Simon et al. 2003). In the vicinity of a plate boundary, such as in the Fiji-Tonga region, eastern Asia, western United States and the surrounding oceans, triplication data are used to study the mantle velocity structures: discontinuity depths, velocity jump across the discontinuities and lateral variation of velocity near a plate boundary (Helmberger and Wiggins 1971; Wiggins and Helmberger 1973; Burdick and Helmberger 1978; Grand and Helmberger 1984b; Houard and Nataf 1993; Brudzinski et al. 1997; Brudzinski and Chen 2000; Brudzinski and Chen 2003; Chen and Brudzinski 2003). Triplication studies also presented the detail structure of a certain discontinuity, such as the velocity and density near a discontinuity, the sharpness of a discontinuity, the slab effects on a discontinuity, and the existence of the 520-km discontinuity (Cummins et al. 1992; Neele 1996; Melbourne and Helmberger 1998; Tseng and Chen 2004, 2008; Obayashi et al. 2006; Chen and Tseng 2007).

The challenges of using upper mantle triplication data lie in the difficulties to compile a record section sampling various depths of the mantle. As a result, earlier studies had to rely on the collection of seismic data covering a large azimuthal range of the sampling region (Wiggins and Helmberger 1973; Burdick and Helmberger 1978; Given and Helmberger 1980; Grand and Helmberger 1984b; LeFevre and Helmberger 1989; Brudzinski and Chen 2003) and to use both S triplication and SS triplication to increase data coverage (Grand and Helmberger 1984a). Recent seismic arrays and networks, such as the Southern California Array, the Kaapvaal Array, US Array, rapidly improve seismic coverage and make it possible to compile dense seismic observations in a small azimuthal range, minimizing the effects of lateral variation of seismic structure (Walck 1984; Zhao et al. 1999; Simon et al. 2002, 2003). Recent development in mineral physics also makes it possible to quantitatively predict characteristic features of mantle properties based on the experimental results in the laboratory. These developments, thus, provide an excellent opportunity for constraining mantle properties and their associated composition and temperature. In particular, modeling the upper mantle triplication data could provide a unique tool for inferring seismic anisotropy as a function of depth in the upper mantle.

In this paper, we first review the wave propagation of the triplicated phases and key seismic features that can be studied using the triplicated phases. We present examples with one for a shallow event and other for two deep events in Sect. 2. We discuss how those key features play an important role in constraining mantle composition and temperature in Sect. 3, the potential of upper mantle triplication data for further studying some other important features of the mantle: the existence of double 660-km discontinuities, existence

of low-velocity channels near major discontinuities and anisotropy varying with depth in Sect. 4, and challenges of the upper mantle triplication study and its connection to other approaches in Sect. 5. Most of the review in Sects. 2 and 3 uses the examples presented in our two previous papers: Wang et al. (2006, 2008).

2 Seismic Triplicated Phases

2.1 Shallow Events

For shallow events, several seismic phases are present in the distance range of 10°–30°: the direct phase traveling in the lithospheric lid (AB branch), the reflection off the 410-km discontinuity (BC branch), the wave traveling in the transition zone (CD branch), the reflection off the 660-km discontinuity (DE branch), the wave traveling below the 660-km discontinuity (EF branch) and the wave traveling in the low velocity zone (CG branch) when a low velocity zone is present (Fig. 1a). The travel time curves of these various branches of the seismic phases are shown in Fig. 1b for the case of the shear wave propagation in a velocity model with a low velocity zone beneath the lithospheric lid.

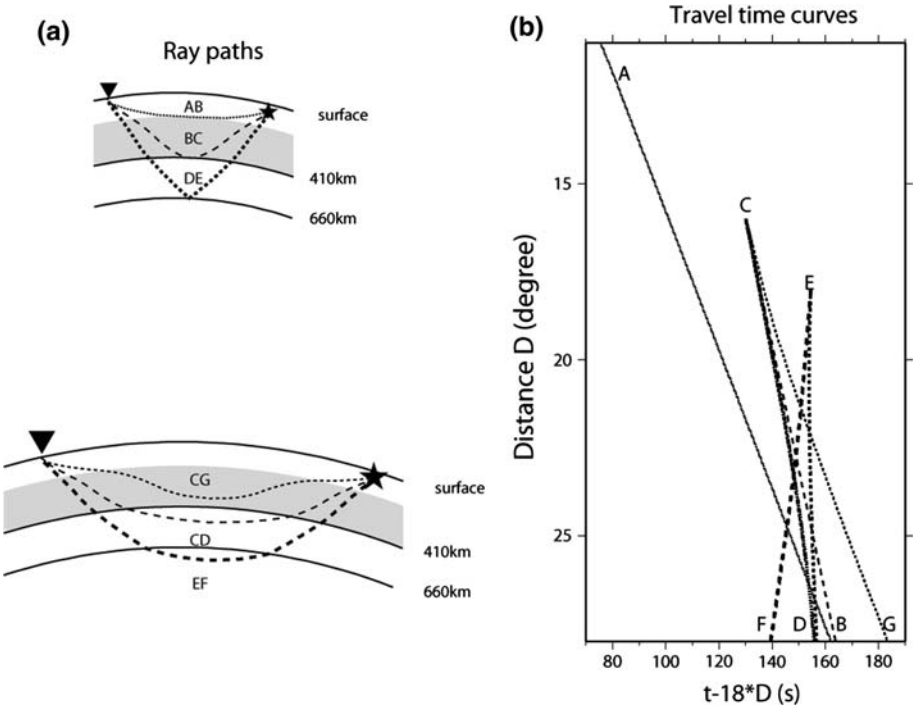

Fig. 1 **a** Ray paths (upper for an epicentral distance of 15°; below for an epicentral distance of 24°) and **b** travel time curves of the triplication in the upper mantle for a source depth of 30 km. The *shaded regions* in **a** represent the low velocity zone. AB branch is the direct wave propagating above the low velocity zone; BC is the reflection off the 410 km discontinuity; CG is the wave traveling in the low velocity zone; CD is the wave traveling in the transition zone; DE is the reflection off the 660-km discontinuity; and EF is the wave traveling below the 660-km discontinuity (from Fig. 2 in Wang et al. 2008)

The amplitude change of the AB phase with distance is sensitive to the presence or absence of a low velocity zone below the lithospheric lid, as well as the onset depth of the low velocity zone. The presence of a low velocity zone would create a shadow zone for the AB branch and generate weak direct arrivals. The onset distance of the observed weakened direct arrivals is controlled by the onset depth of the low velocity zone. A shallower onset depth of the low velocity zone would make the AB branch disappear at a smaller distance. The seismic effects of the low velocity zone are illustrated in Fig. 2a. Note that the synthetics for the model with a low velocity zone display weakened AB phases at epicentral distances larger than 15°. The travel time differences between the AB and BC branches and between the AB and CD branches are sensitive to the velocity reduction in the low velocity zone and the depth of the 410-km discontinuity.

The travel time of the AB branch is also sensitive to seismic velocity structure in the shallow mantle and can be used to place constraints on the presence of a high-velocity lithospheric lid and the seismic structures in the lid. The effects of mislocation of the events have to be carefully considered when one employs the absolution travel times to constrain the seismic structures. Triplication data would also minimize the effects of the mislocation of the earthquakes by using the relative timing and waveform of the different branches of the seismic phases. The effects of a lithospheric lid are illustrated in Fig. 2b. Note that, when a high-velocity lithospheric lid is present, the AB phases arrive earlier and

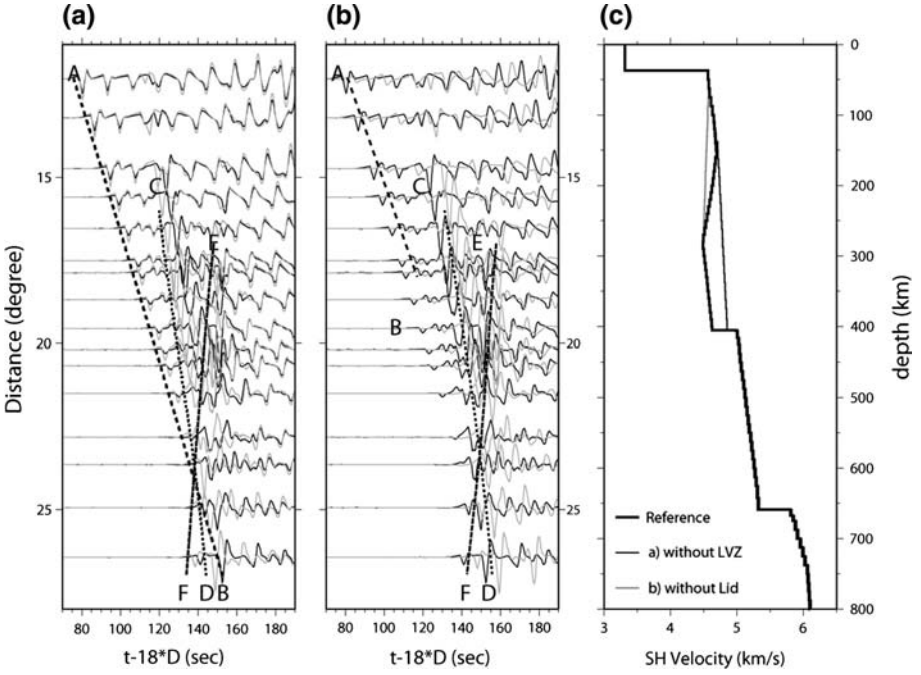

Fig. 2 Comparisons of synthetic tangential displacements for a source depth of 30 km, calculated using a reference SH velocity model (*black traces*) and two testing models perturbed from the reference model (*gray traces*): **a** without a low velocity zone and **b** without a lithospheric lid, along with predicted travel time curves of the three branches of the seismic phases (*dashed lines*). Models are shown in (**c**) and labeled accordingly with the synthetics panels

the differential travel times between the AB phases and other branches of the phases are larger.

For the same reasons, the absolute and differential travel times between other branches of the phases can be used to constrain seismic structures at various depth ranges in the mantle. For example, the travel time difference between the CD and DE branches is sensitive to the depth of the 660-km discontinuity and the velocity structure above the 660-km discontinuity. The travel time difference between the CD and EF branches is sensitive to the seismic velocity in the transition zone, the velocity jump across the 660-km discontinuity and the depth of the 660-km discontinuity. The absolute S wave velocities and the velocity gradient in the transition zone can be constrained by the absolute travel time and the move-out of the CD branch. A larger velocity would make the CD branch arrive earlier, and a larger velocity gradient would cause a larger move-out of the CD branch. The velocity jump across the 660-km discontinuity can be constrained by the travel time difference between the CD and EF branches. A larger velocity jump would make the CD branch arrive relatively later or the EF branch relatively earlier, i.e., a larger travel time difference between the CD and EF branches. A smaller velocity jump would do the opposite.

We show an example of using the triplication data and the multiple reflections inside the crust of shallow events to constrain seismic structure in the crust and the upper mantle. The sampling region of the seismic data is the crust and the upper mantle beneath southern Africa (Fig. 3). The crust structure in this region is constrained using the SH multiple reflections inside the crust (the wavelets pointed to by the arrow in Fig. 4b), and the P and SH velocity structures of the upper mantle in this region are constrained using the triplicated phases recorded by the Kaapvaal Seismic Array in the epicentral distance range of 11°–27° for a shallow event occurring in southern Africa. The dense coverage of the Kaapvaal Array provides good sampling coverage for the entire depth range in the upper mantle, from about 125 km deep at an epicentral distance of 11° to about 750 km deep at 27°.

Three branches of triplication and the multiple reflections inside the crust are clearly identifiable in the tangential components of the data. The AB branch starts to appear weak at a distance of about 20° and becomes indiscernible at larger distances. The EF phase crosses over the CD phase at about 23.5° (Fig. 4a). A low velocity zone beneath the high-velocity lid is needed to explain the amplitude decrease of the AB branch with increasing epicentral distance and its disappearance at the distances larger than 20°. The termination distance of the AB branch suggests that the onset depth of the low velocity zone is 150–210 km deep. The differential travel times between the AB and CD branches suggests a minimum velocity reduction of -5% in the low velocity zone. The absolute S wave velocities, the velocity gradient in the transition zone, and the S velocity jump across the 660-km discontinuity are also well constrained by the absolute travel time and the move-out of the CD branch, and the travel time difference between the CD and EF branches. The S velocity inside the crust is constrained by the travel time difference between the multiple reflections in the crust.

Only two branches of triplication are clearly identifiable in the observed vertical displacements. The AB branch can be clearly observed in the data until at a distance of about 17° and becomes indiscernible at larger distances (Fig. 4b). A low velocity zone for the P waves with a minimum velocity reduction of -2% is also required to satisfy the travel time difference between the AB and CD branches. The P and SH data also indicate different P to S velocity ratios in the lithospheric lid and in the transition zone. The reflection off the 660-km discontinuity and the wave traveling below the 660-km discontinuity, while it is clear

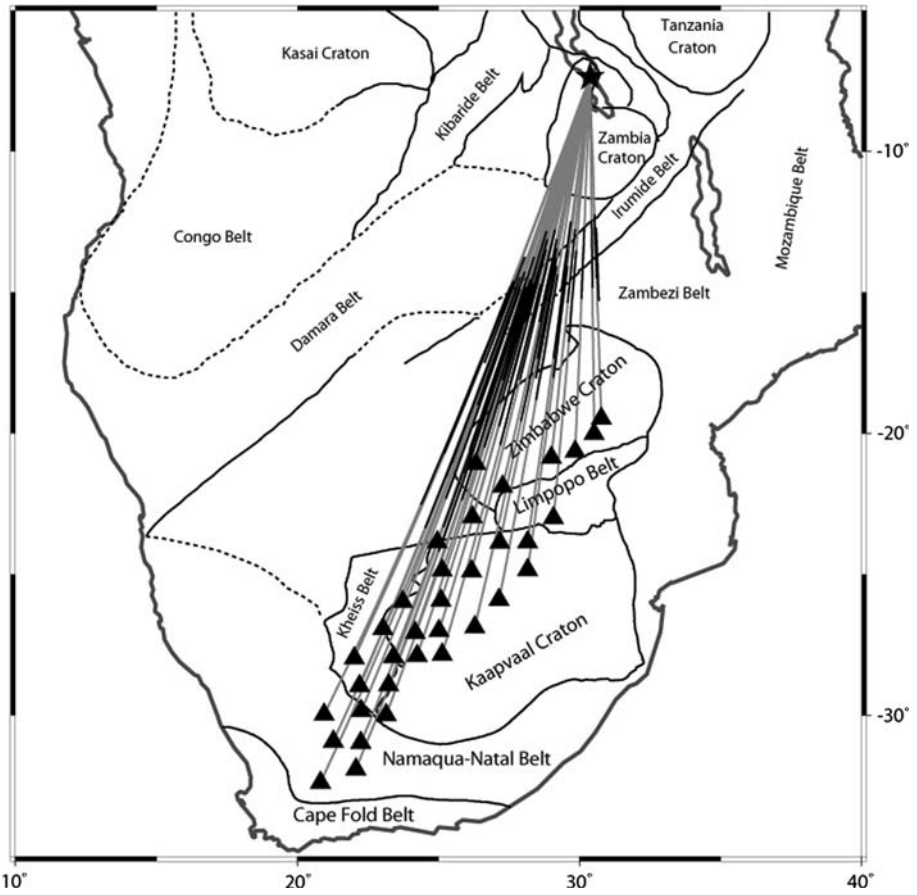

Fig. 3 Map showing great circle paths from seismic event (*star*) to stations (*triangles*), with the *black* segments indicating the portions that the BC branch (defined in Fig. 2) travels below the lithospheric lid, as well as the geologic provinces in southern Africa. The original time of the earthquake is 1997/09/21/18:16:27 and the event depth is 30 km (adapted from Fig. 1 in Wang et al. 2008)

in the SH wave data, cannot be recognized in the P wave data. This suggests a P velocity jump smaller than 5% across the 660-km discontinuity. The large SH velocity jump and the small P velocity jump suggest a bulk sound velocity decrease across the 660-km discontinuity.

2.2 Deep Events

For deep events, three triplicated seismic phases near a discontinuity (Fig. 5) are present at an epicentral distance range of 10°–30°: the wave propagating above the discontinuity (AB branch), the reflection off the discontinuity (BC branch) and the wave traveling below the discontinuity (CD branch). The travel time curves of these three branches of the seismic phases are shown in Fig. 5b for the case of the shear wave propagation in PREM (Dziewonski and Anderson 1981).

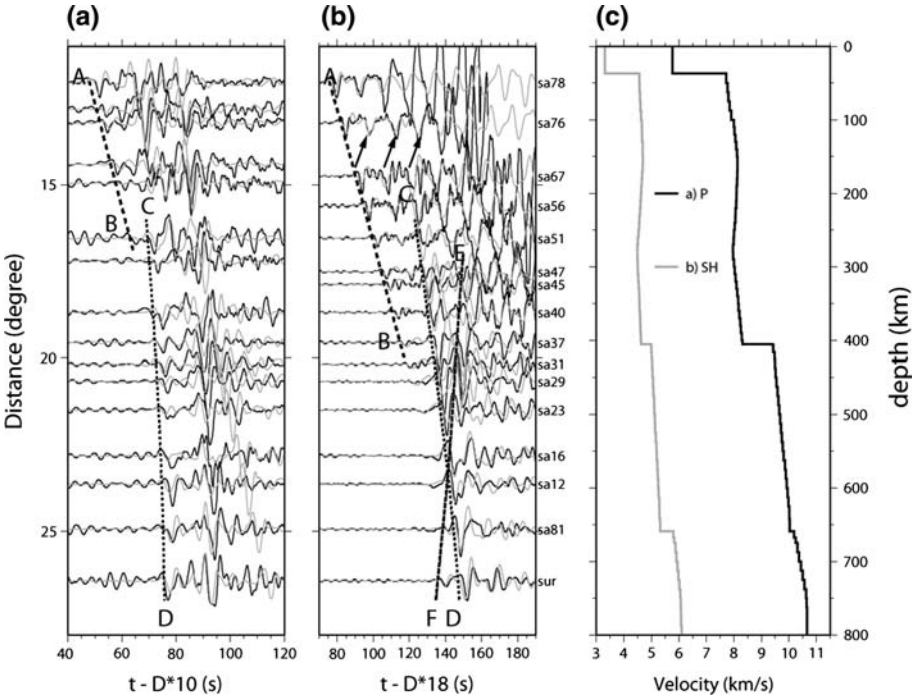

Fig. 4 Comparisons of observed **a** vertical and **b** tangential displacements for the seismic waves sampling the upper mantle beneath southern Africa (*black traces*) and synthetic waveforms (*gray traces*) calculated using the best fitting models, along with predicted travel time curves of different seismic phases (*dashed lines*). The best fitting models are shown in (**c**). Waveforms are plotted in absolute amplitude (from Figs. 5a, 3a in Wang et al. 2008)

We discuss the wave propagation for events near the 660-km discontinuity, as an example. The same approach can also be applied to other discontinuities. Since the ray paths of these three phases are very close in the shallow proportion of the mantle (Fig. 5a), the travel time difference and waveform between these phases are primarily sensitive to the velocity structure near the 660-km discontinuity. Waveforms of the triplication data thus provide powerful constraints on the detailed features of the discontinuity.

The termination distance of the AB branch is sensitive to the velocity gradient above the 660-km discontinuity. The larger the velocity gradient above the discontinuity, the smaller the termination distance of the AB branch. This propagational effect is illustrated in the comparisons of synthetics of two models with different velocity gradients above the 660-discontinuity (Fig. 6a). A model with the PREM velocity gradient above the 660-km discontinuity predicts the persistence of the AB phase to large distances (>27°), while a model with a larger velocity gradient [0.0024 (km/s)km] above the 660-km discontinuity would make the AB phase terminated at a closer epicentral distance of about 23° (Fig. 6a).

The travel time difference between the AB and CD branches and the cross-over distances between the AB and CD branches are sensitive to the velocity jump across the 660-km discontinuity. A larger velocity jump would generate a larger differential travel time between the AB and CD branches and a closer cross-over distance, while a smaller velocity jump would do the opposite. These propagational effects are illustrated in the comparisons of synthetics calculated using two different velocity jumps across the 660-km discontinuity

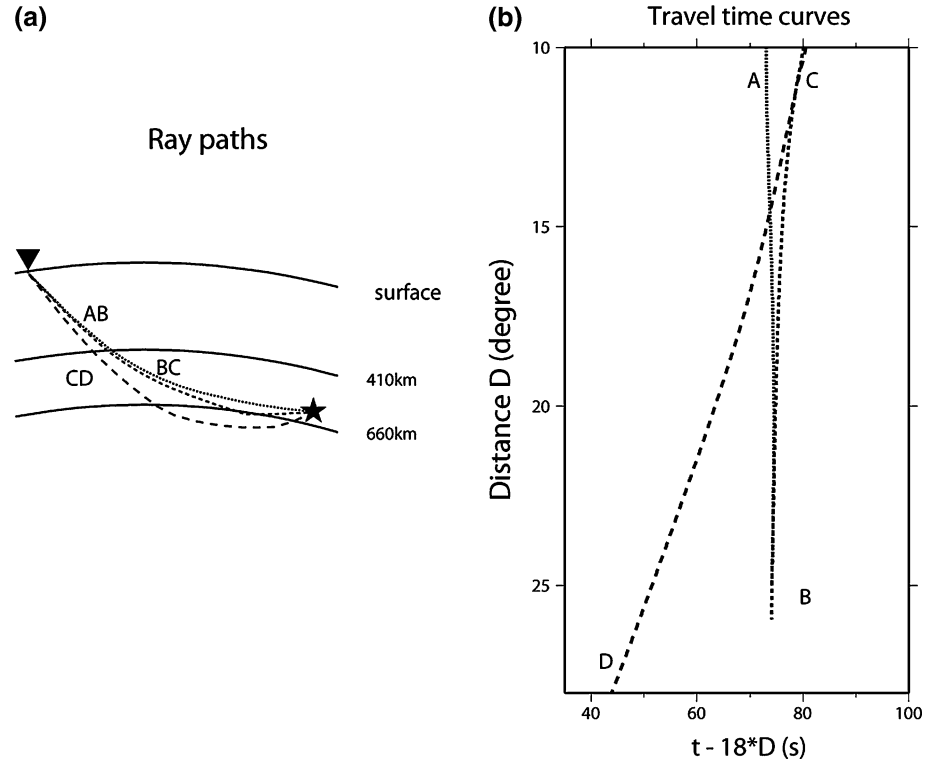

Fig. 5 **a** Ray paths and **b** travel time curves of the triplication near the 660-km discontinuity for a source depth of 597 km. The AB branch is the direct SH wave propagating above the discontinuity; the BC branch is the reflection off the discontinuity; and the CD branch is the seismic wave traveling below the discontinuity (from Fig. 2 in Wang et al. 2006)

(Fig. 6b). Synthetics for the model with a smaller velocity jump across the 660-km discontinuity exhibit a smaller travel time difference between the AB and CD branches and a closer cross-over distance between the two branches (Fig. 6b).

The move-out of the CD branch is sensitive to the velocity gradient below the 660-km discontinuity and the depth extent of the gradient. The effects of the velocity gradient below the 660-km discontinuity are clearly illustrated in the comparisons of the synthetics for models with different velocity gradients and depth extents of the velocity gradient below the 660-km discontinuity. Note that, synthetic waveforms calculated using a smaller velocity gradient below the 660 km discontinuity exhibit a different move-out of the CD phase (Fig. 7a). Synthetics calculated with a shallower depth extent show a change of the move-out of the CD phases at a closer epicentral distance of 18° (Fig. 7b).

We present two examples of using the triplication data for deep events to constrain the detailed seismic features near the 660-km discontinuity, with one sampling the South American and the other sampling North East Asia. Seismic data recorded in the two PASSCAL experiments for event 1 constitute a good record section sampling the seismic structure near the 660-km discontinuity beneath South America (black traces, Fig. 8a), while those recorded in the New Chinese Digital Seismic Network (NCDSN) for event 2 constitute a good record section sampling the seismic structure near the 660-km discontinuity beneath North East Asia (black traces, Fig. 8b).

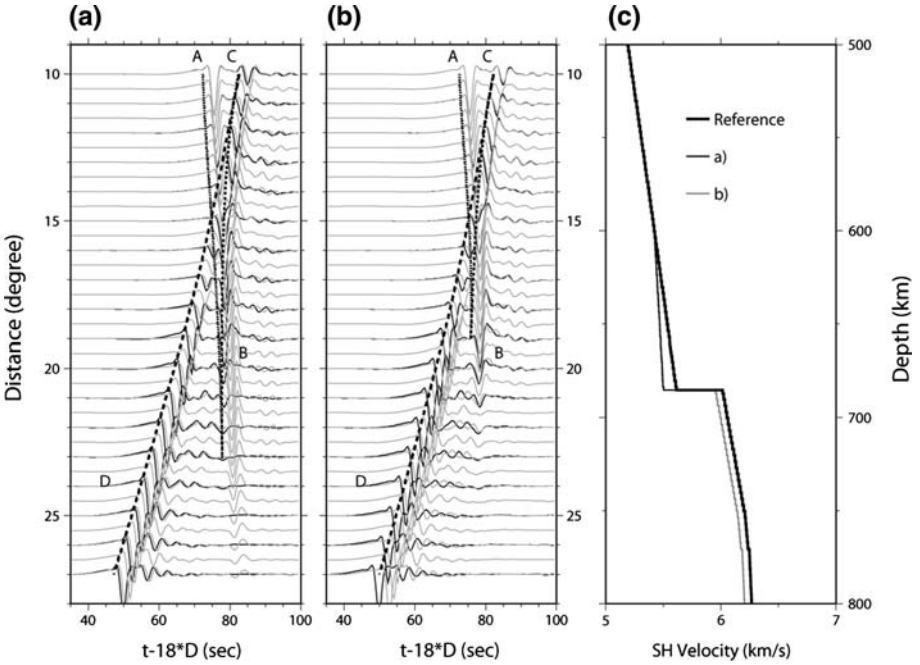

Fig. 6 Comparisons of synthetic tangential displacements for a source depth of 597 km calculated using a reference SH velocity model (*black traces*) and two testing models perturbed from the reference model (*gray traces*): **a** with a smaller velocity gradient above the 660-km discontinuity and **b** with a smaller jump across the 660-km discontinuity, along with predicted travel time curves of the three branches of the seismic phases (*dashed lines*). Models are shown in (**c**) and labeled accordingly with the synthetics panels

For the South American event, three branches of triplication are clearly identifiable in the tangential displacements observed at the distance range of 10°–27°. The AB branch turns about 600 km deep in the transition zone at an epicentral distance of 10° and starts to diffract at the top of the 660-km discontinuity at an epicentral distance of about 20°. The CD phase crosses over the AB phase at about 15° and samples the top of the lower mantle to a depth of 820 km at 27°. The AB branch can be clearly observed in the data after the cross-over (see data at stations PTMB, NAVB) until at a distance of about 20° and becomes indiscernible at stations TRIB, AGVB, OLIB, RIFB and CACB at larger distances (black traces, Fig. 9a).

While the velocity jump crosses the 660-km discontinuity and the velocity gradient below the discontinuity in PREM can well explain the differential travel times between the AB and CD phases and the move-out of the CD phase in the data, a larger velocity gradient above the 660-km discontinuity and a deeper 660-km discontinuity are needed to explain the termination distance of the AB phase and the differential travel times between the AB and BC phases in the seismic data. A larger velocity gradient above the discontinuity would make the AB branch terminate at a closer distance as observed in the data; and a deeper discontinuity would predict a larger travel time difference between the AB and BC branches. The best-fitting model has a velocity gradient of 0.0024 (km/s)/km above the discontinuity and a deeper 660-km discontinuity at 685 km (Fig. 9c). Synthetics of this best-fitting model match well the termination distance of the AB branch and the travel time difference between the AB and BC branches (Fig. 9a).

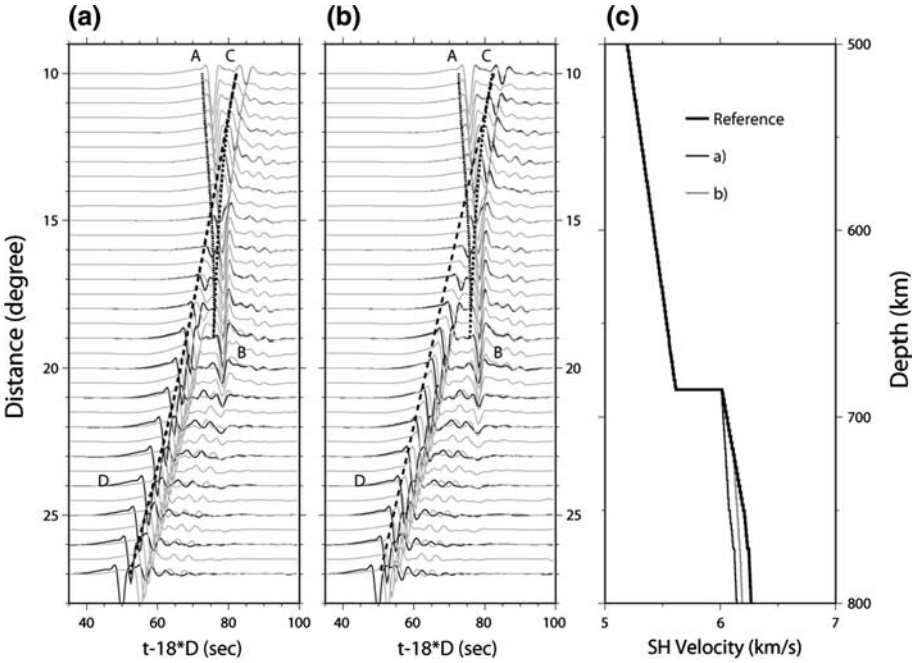

Fig. 7 Comparisons of synthetic tangential displacements for a source depth of 597 km calculated using a reference SH velocity model (*black traces*) and two testing models perturbed from the reference model (*gray traces*): **a** with a smaller velocity gradient below the 660-km discontinuity and **b** with a smaller depth extent of the large velocity gradient below the 660-km discontinuity, along with predicted travel time curves of the three branches of the seismic phases (*dashed lines*). Models are shown in (**c**) and labeled accordingly with the synthetics panels

For the event in Asia, three branches of triplication are clearly identifiable in the distance range of 10°–35°. The AB branch turns about 480 km deep in the transition zone at an epicentral distance of 10° and starts to diffract at the top of the 660-km discontinuity at an epicentral distance of about 30°. The AB branch can be clearly observed at stations HNS, TIY, HEF, WZH, WHN, NNC, CNS, GTA, and becomes indiscernible at stations GZH, CD2, GUL, SZN at distances greater than 30° (Fig. 9b). The CD phase crosses over the AB phase at about 19° (Fig. 9b) and samples the top of the lower mantle to a depth of about 910 km at 35°.

Different from the data sampling the South American, the persistence of the AB phases to large epicentral distances for the data sampling North East Asia requires a PREM-like velocity gradient above the 660-km discontinuity. The PREM-like velocity gradient below the discontinuity also well explains the move-out of the CD phase in the data. But, the differential travel times between the AB and CD phases suggest a large velocity jump across the 660-km discontinuity. The best-fitting model has PREM velocity gradients in the transition zone, a velocity jump of 0.53 km/s across the discontinuity, a large PREM-like velocity gradient extending 80 km below the 660-km discontinuity and a deeper discontinuity at 730 km (Fig. 9c). Synthetics calculated based on the best-fitting model fit the observed travel time differences between the AB and BC branches, cross-over distance, move-out of the CD phase and overall waveforms well (Fig. 9b).

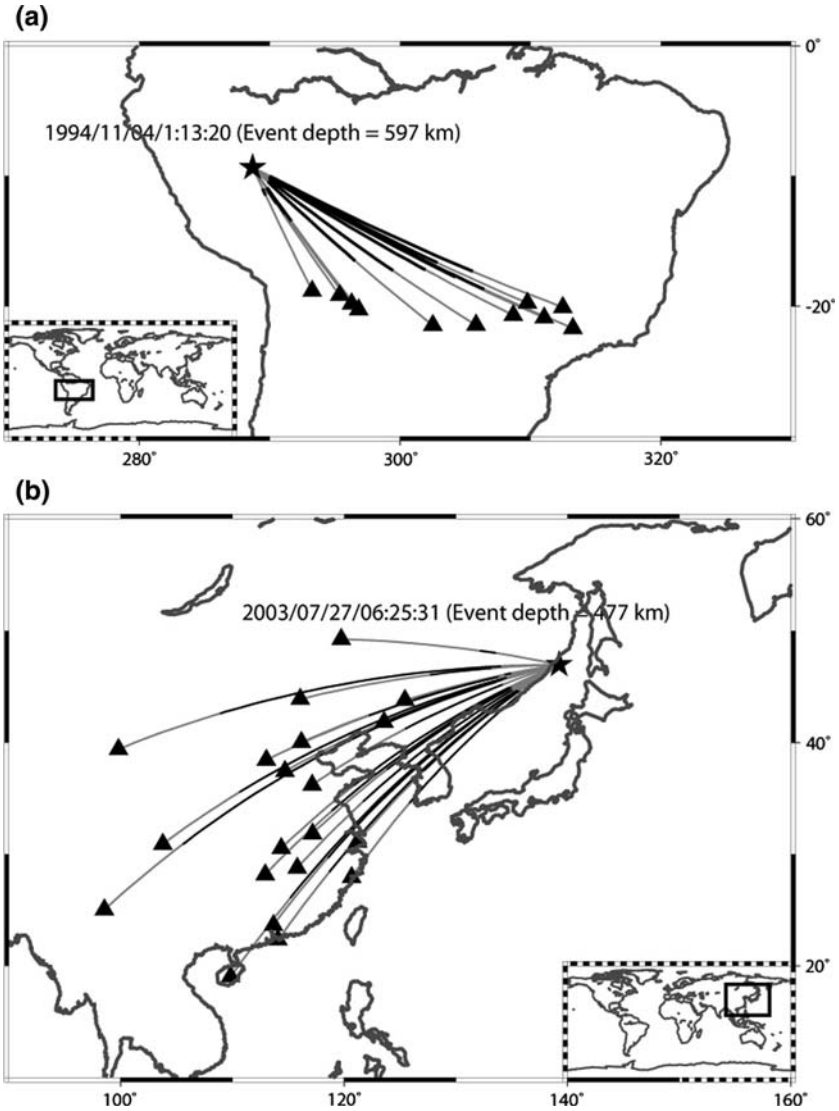

Fig. 8 Great circle paths from seismic events (*stars*) to array stations (*triangles*), with the *black* segments indicating the portions that the CD branch travels below the 660-km discontinuity, in two study regions: **a** South America (event 1) and **b** North East Asia (event 2) (adapted from Fig. 1 in Wang et al. 2006)

3 Importance of the Key Seismic Features Constrained by the Triplication Data to the Understanding of Mantle Composition and Dynamics

The following detailed seismic features can be studied using the upper mantle triplication data: the existence of a lithospheric lid, the existence of a low velocity zone, P/S velocity ratio at various depths, and detailed features associated with the major discontinuities in the mantle. We discuss the importance of these features to the understanding of mantle composition and dynamics.

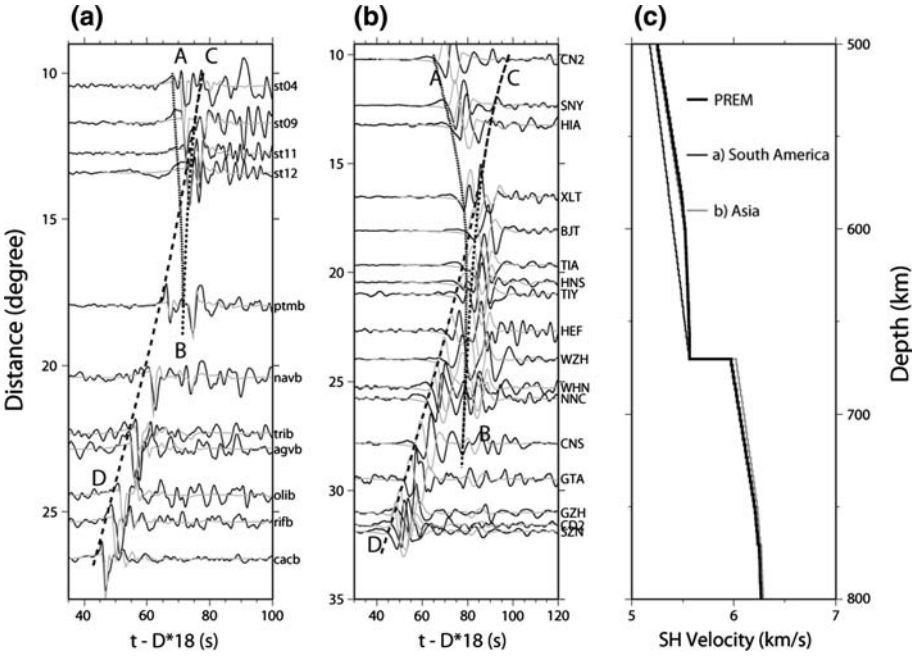

Fig. 9 Comparisons of observed tangential displacements (*black traces*) for the seismic waves sampling the transition zone **a** beneath South America and **b** beneath North East Asia and synthetic waveforms (*gray traces*) calculated using **a** best fitting velocity model for South America and **b** best fitting velocity model for North East Asia, along with predicted travel time curves of the three branches of the seismic phases (*dashed lines*). Models are shown in (**c**) and labeled accordingly with the synthetics panels. Station travel time corrections are made for following stations: TRIB (−1.5 s), OLIB (−1.0 s), RIFB (−0.5 s), CN2 (2 s), SNY (2 s), TIA (2 s), HNS (2 s), TIY (2 s), GTA (2.5 s), based on the observations from another events. (from Figs. 3b, 5b in Wang et al. 2006)

3.1 Lithospheric Lid, Low Velocity Zone and P/S Velocity Ratio

The existence of a lithospheric lid and depth extent of the lithospheric lid are important to the understanding of tectonics in the region. The existence of a low velocity zone and the magnitude of the velocity reductions in the low velocity zone would place important constraints on temperature and existence of partial melt beneath the lithosphere. The seismic structures, especially when both P and S wave velocities are available, would place important constraints on the composition and thermal profiles in the mantle. We take the velocity profiles beneath Africa as an example. The low velocity zone beneath the lithospheric lid can be explained by a high temperature gradient or partial melt. In the absence of partial melt, a temperature gradient of about 6°C/km in the depth range of 150–275 km (Fig. 10d) is needed to satisfy the minimal shear velocity reduction of −5% inferred for the low velocity zone beneath southern Africa. Such a temperature gradient would indicate that the mantle density in the low velocity zone is about 4% smaller than the density in lithospheric lid. In the presence of partial melt, the presence of water or other volatile elements would be required in the depth range of the low velocity zone to suppress the solidus, as the solidus of the dry peridotite (Zhang 1994) would be higher than the inferred temperature, even with a temperature gradient of 6°C/km (Fig. 10d). The presence of a low-density anomaly beneath the lithospheric lid is consistent with the observed high heat

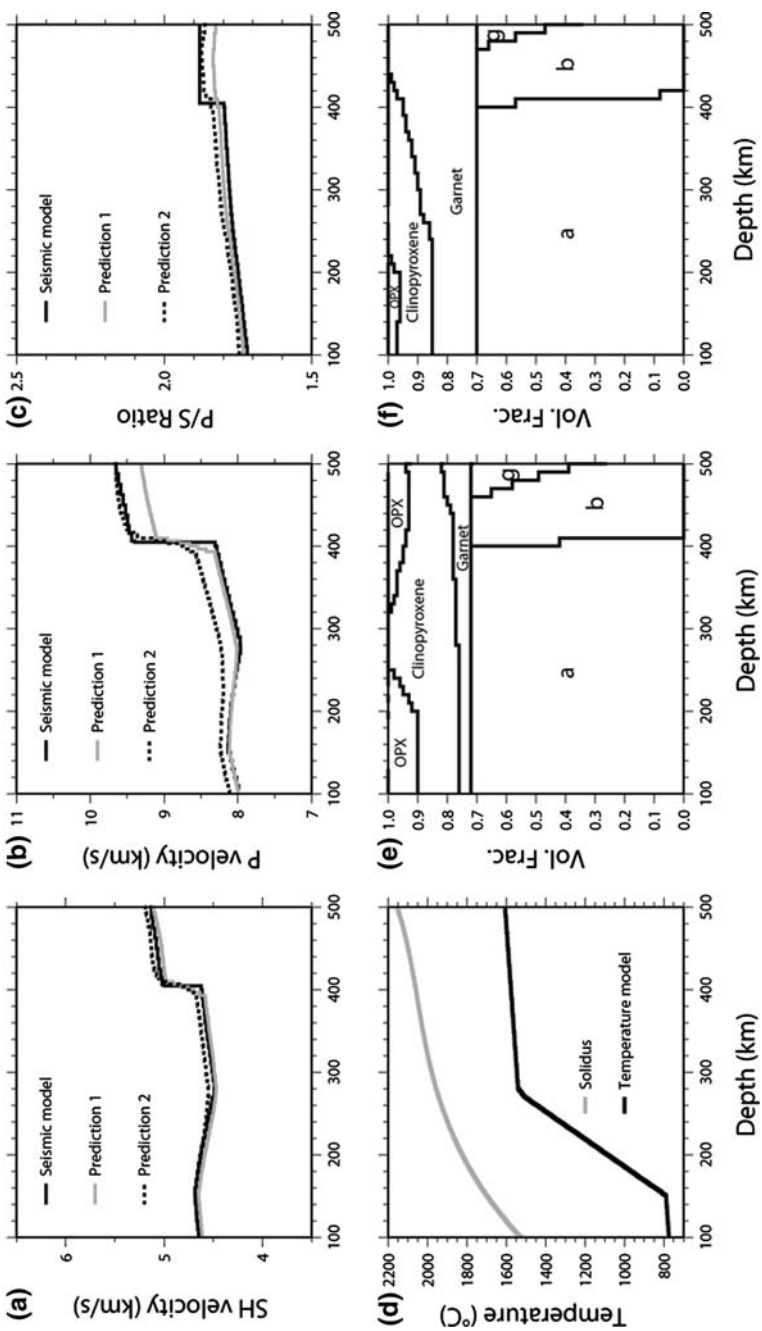

Fig. 10 **a–c** Comparisons between seismic velocity models and the predictions based on two mantle compositional models, **a** for S wave velocities, **b** for P wave velocities and **c** for P to S velocity ratios; **d** thermal model and the solidus for the anhydrous Peridotite (Zhang 1994) and **e–f** mineralogical models predicted based on the thermal model in (**d**) and two mantle compositional models with Al contents of 1% (**e**) and 4% (**f**). α denotes olivine; β wadsleyite; γ ringwoodite; OPX orthopyroxene; and CPX clinopyroxene (from Fig. 8 in Wang et al. 2008)

flow, localized uplift and broad geoid anomalies in the region of the "African Superswell". The shallow high temperature, low-density, buoyancy generates high heat flow on the ocean floor of the "African Superswell" (Nyblade and Robinson 1994) and large uplifts in the region with little localized geoid anomaly. The geoid anomaly observed in a broader region of Africa may be attributed to the large-scale seismic anomalies in the lower mantle (Wang and Wen 2007).

The different P to S velocity ratios between the lithospheric lid and the transition zone can be explained by a difference in aluminum content of the mantle composition in the two depth regions. A higher aluminum content would result in more garnet and less clinopyroxene and orthopyroxene (Fig. 10f). Because the bulk modulus of garnet is much larger than those of clinopyroxene and orthopyroxene, and the shear modulus of garnet is only slightly larger than those of clinopyroxene and orthopyroxene, a higher aluminum content would cause a higher P wave velocity, but a similar S wave velocity and, thus, a higher P to S velocity ratio. In the lithospheric lid, a compositional model with an aluminum content of 1% can explain the absolute seismic velocities and the P to S velocity ratio. A lower aluminum content results in more clinopyroxene and orthopyroxene and less garnet (Fig. 10e) and thus a lower P/S velocity ratio (Fig. 10c) in the lithospheric lid. In the transition zone, the higher P to S velocity ratio requires a higher aluminum content of 4%. A higher aluminum content results in more garnet and less clinopyroxene and orthopyroxene in the transition zone, and thus a higher P to S velocity ratio (Fig. 10c). The lower Al content inferred for the lithospheric lid could result from the depletion of the basaltic component of the mantle composition beneath the old continental nuclei, consistent with the tectonosphere hypothesis beneath the continental cratons (Jordan 1978).

3.2 Detailed Features of a Seismic Discontinuity in the Mantle

Velocity jumps across a discontinuity, velocity gradients above and below a discontinuity, and depth extent of the velocity gradients are among the most diagnostic indicators to mantle mineralogy, composition and temperature. We illustrate the importance of their constraints, taking the models inferred for the 660-km discontinuities beneath South America, North East Asia and Africa, as examples.

The velocity gradient above the 660-km discontinuity beneath North East Asia can be explained by the temperature and pressure dependence of elastic properties of the major phases in the transition zone (ringwoodite + garnet + Ca-perovskite; Fig. 11c). But the velocity gradient above the 660-km discontinuity beneath South America is larger than what is expected for the temperature and pressure dependence of elastic properties of the major phases, and would require existence of ilmenite (Fig. 11b). Because the shear wave velocity of ilmenite is larger than that of garnet, increasing volume fraction of ilmenite results in a large velocity gradient above the 660-km discontinuity. The garnet–ilmenite transformation occurs in low temperature or in compositions with a lower aluminum content. The existence of ilmenite beneath South America and the absence of ilmenite beneath North East Asia would suggest that, beneath South America, mantle temperature (at 660 km) is about 100°C/km lower (assuming same Al contents in the two regions) or the Al content is 1.2% lower (assuming same temperatures in the two regions).

The existence of a large velocity gradient below the 660-km discontinuity is due to the effect of the phase transformation from garnet to perovskite. The garnet–perovskite transformation can be characterized by a first-order transformation at about 660 km deep followed by a gradual transformation from garnet to perovskite over a certain pressure range. The first-order transformation results in a first-order discontinuity. Because

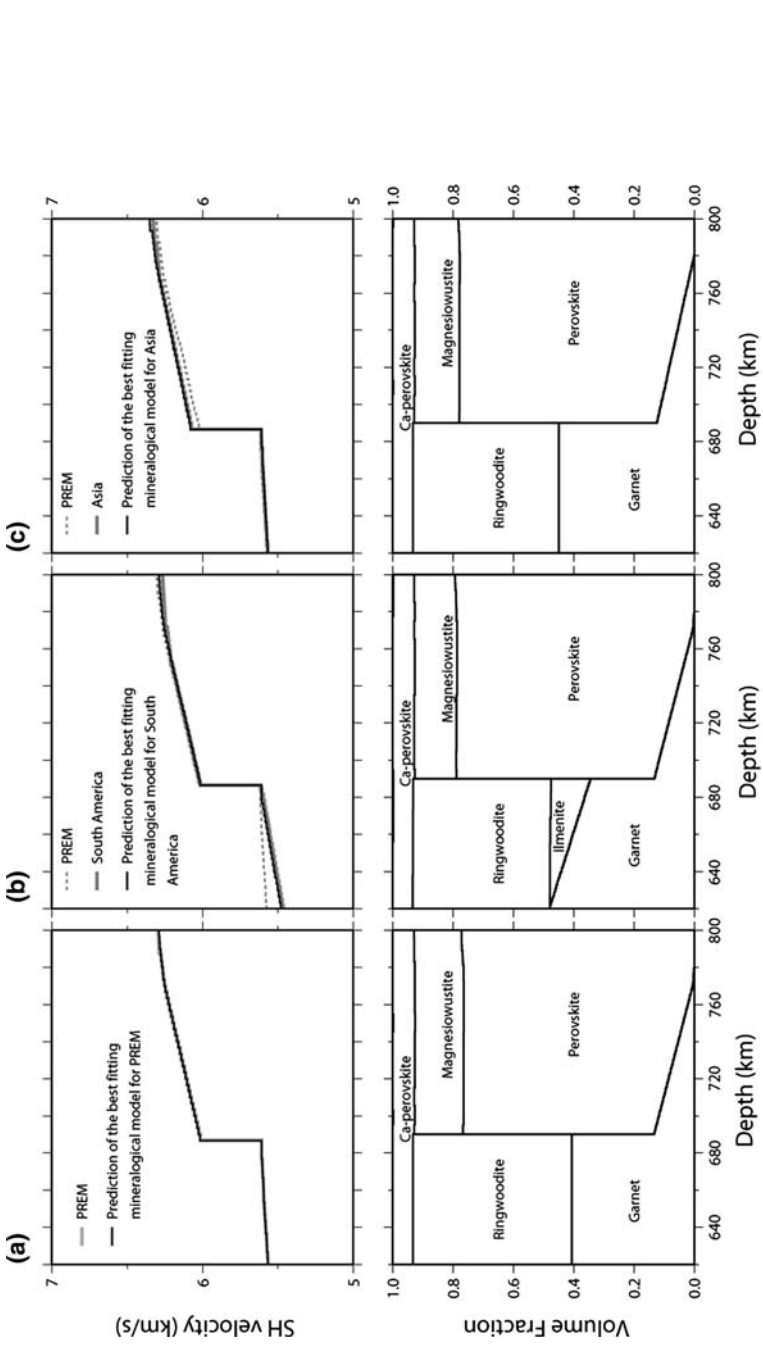

Fig. 11 (*Top*) Comparisons between **a** PREM, **b** best fitting model for South America and **c** best fitting model for northeast Asia, and predicted velocity structures based on three mineralogical models shown in the bottom. Velocity models are calculated on the basis of measured elastic properties, relative volume fractions of these phases, and an adiabatic temperature gradient of 0.7°C/km. PREM is plotted as reference. (*Bottom*) Volume fractions of major mineral phases as a function of depth in three mineralogical models. The phase transformations from ringwoodite to perovskite plus magnesiowustite and from garnet to perovskite are assumed to occur in a same depth in the calculation (from Fig. 13 in Wang et al. 2006)

perovskite has a higher velocity than garnet, the subsequent gradual transformation results in a large velocity gradient below the 660-km discontinuity. The pressure range of the gradual transformation, or the depth extent of the high velocity gradient below the first-order discontinuity, is sensitive to the aluminum content of mantle composition. The gradual transformation for a composition with a higher Al content would occur over a larger pressure range, and thus result in a larger depth extent of the large velocity gradient.

The depth extent of the large velocity gradient below the 660-km discontinuity (about 80 km, Fig. 11b, c) indicates a mantle composition with an aluminum content of 3.4% in the top of the lower mantle.

The velocity jumps across the 660-km discontinuity is sensitive to the relative fractions of garnet and olivine components in mantle composition. For example, in order to maintain the velocity jump across the discontinuity and the depth extents of the high velocity gradient below the discontinuity to be similar to PREM, in the presence of ilmenite, a larger volume fraction of garnet than the pyrolite model is needed beneath South America (Fig. 11b). The larger shear velocity jump across the 660-km discontinuity beneath North East Asia would also require a larger volume fraction of garnet present. Perhaps, more interestingly, the PREM-like SH velocity jump and a small P velocity jump across the 660-km discontinuity beneath Africa (Fig. 4c) suggests a bulk sound velocity decrease of 3.4% across the 660-km discontinuity. Current estimates of elastic properties of mantle phases are incompatible with this magnitude of bulk sound velocity decrease. Such a large decrease of bulk sound velocity would require the bulk modulus of perovskite to be similar to those of ringwoodite and garnet at the pressure and temperature conditions around the 660-km discontinuity, a result pointing to the need of further experimental or theoretical studies of mineral behaviors near the 660-km discontinuity.

Low temperature or low aluminum content is consistent with presence of a subducting slab. Since both sampling regions are in the vicinity of subducting slabs, if the larger velocity gradient above the 660-km discontinuity beneath South America is caused by a lower mantle temperature, the South America sampling region is closer to a subducting slab than the North East Asia sampling region; if the larger velocity gradient is caused by a lower aluminum content, since the same depth extent of the large velocity gradient below the 660-km discontinuity indicates a uniform composition in the top of the lower mantle in the two regions, the different aluminum contents above and below the discontinuity could indicate a stagnant slab above the 660-km discontinuity beneath South America.

4 Outlooks

Modeling array triplication data has potential to constrain several other important seismic features in the mantle: double discontinuities near the 660-km depth, low velocity channels near the major discontinuities, and anisotropy structure varying with depth. Those properties are sensitive to mantle temperature, composition, chemical interaction and diffusion between mantle minerals, and mantle flow.

4.1 Double 660-km Discontinuities

At about 660 km deep, two perovskite-forming transformations occur: with one from ringwoodite and the other from garnet. The phase transformation from ringwoodite to perovskite plus magnesiowustite is endothermic with a negative Clapeyron slope, while that from garnet to perovskite is exothermic with a positive Clapeyron slope. When the

mantle temperature is high, the phase transformation from ringwoodite to perovskite plus magnesiowustite occurs at a lower pressure and the phase transformation from garnet to perovskite occurs at a higher pressure, and vice versa. If these transformations do not interact chemically, they will most likely occur at different pressures and double discontinuities would appear near the 660-km depth. The two perovskite-forming transformations, however, are also controlled by the chemical interactions between them (Wang et al. 2006). The chemical interactions are mostly due to different Al partitioning between different co-existent minerals and the effect of Al on the garnet–perovskite transformation. Depending on the temperature and Al content, the two perovskite-forming transformations could produce various types of double continuities near 660 km depth (Wang et al. 2006).

Triplication data would be useful for constraining existence of double 660-km discontinuities. Double discontinuities, if separated enough, would generate an additional phase after the cross-over of the CD phase (the phase pointed to by the arrow in Fig. 12a).

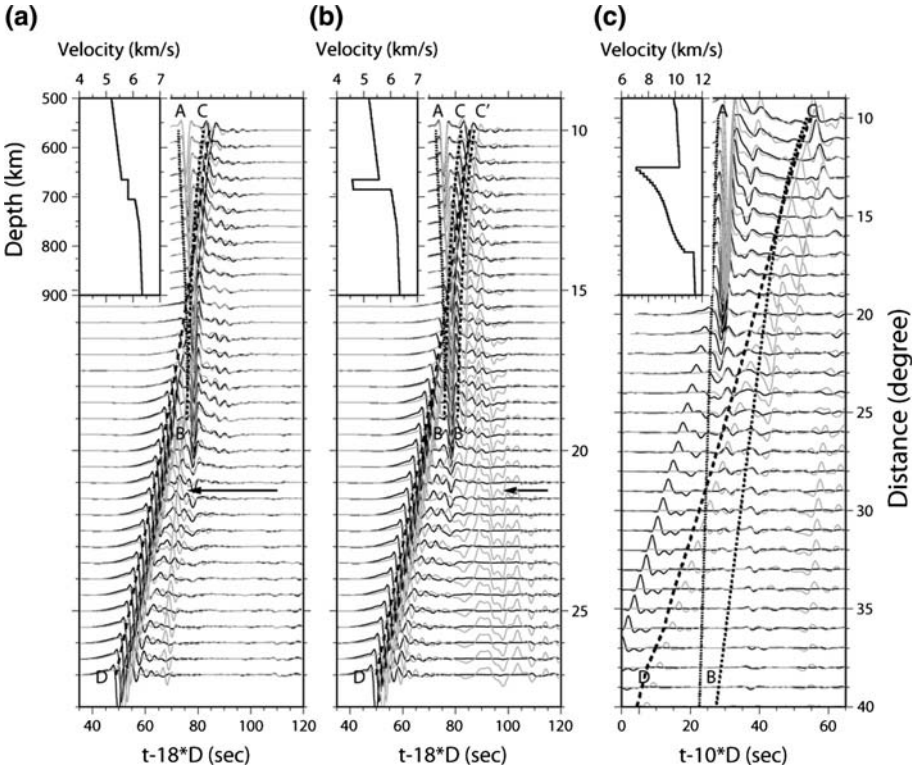

Fig. 12 **a–b** Comparisons of synthetic tangential displacements for a source depth of 597 km, calculated using a reference SH velocity model (*black traces*) and two testing models perturbed from the reference model (*gray traces*): **a** with double discontinuities near the 660-km depth with a depth separation of 40 km, and **b** with a 20 km thick low velocity zone near the 660-km discontinuity, along with predicted travel time curves of the three branches of the seismic phases (*dashed lines*). **c** Comparisons of synthetic vertical displacements for a source depth of 597 km, calculated using a reference P velocity model (*black traces*) and a testing model perturbed from the reference model (*gray traces*) with a 180-km thick gradually changing low velocity zone below the 660-km discontinuity along with predicted travel time curves of the three branches of the seismic phases (*dashed lines*). Models are shown in the upper-left corner of the panels

4.2 Low Velocity Channels Near the Discontinuities

In a two-phase zone during a phase transformation, the effective bulk modulus could be significantly lowered if the pressure of the seismic wave drives a volume-reducing phase transformation. Such effects of relaxation and attenuation by the stress generated during the seismic wave propagation would depend on the comparison between the amount of time required by phase transitions to reach equilibrium and the sampling periods of seismic waves. A recent study by Li and Weidner (2008) showed that softening of the bulk modulus within the two-phase loop of the olivine–ringwoodite transformation is on a timescale of 100 s, based on synchrotron experimental data. They further suggested that, if the amplitude of the pressure perturbation and the grain size are scaled to those expected in the Earth, the compressional-wave velocities within the discontinuities at 410, 520 and 660 km are likely to be significantly lower than otherwise expected. Among the predicted features of the relaxation is existence of low velocity channels near the major discontinuities. A thin low velocity channel above the 410-km discontinuity is also predicted based on the hypothesis of transition zone filter (Bercovici and Karato 2003).

Triplication data would be useful to constrain the existence and properties of the low velocity channels. A thin low velocity channel near the discontinuity would generate reflections off the top and bottom boundaries of the low velocity channel in the close distances (BC and B′C′ phases in Fig. 12b). More diagnostically, it would trap waves at the diffracted distances, producing multiples inside the layer (the wavelets pointed to by the arrow in Fig. 12b). The travel time difference between two reflections is sensitive to the thickness and velocity reduction of the low velocity channel, and can be used to place constraints on these properties.

Triplication data would also be useful for constraining a possible broad low velocity zone below the 660-km discontinuity. Such a low velocity zone is predicted based on the relaxation effect in the broad phase loop of the garnet–perovskite transformation. A broad low velocity zone below the 660-km discontinuity would make the cross-over occur at large distances and produces a decreased AB phase at large distances before the cross-over by the CD phase (Fig. 12c). The negative discontinuity at the top and the positive discontinuity in the bottom would produce strong reflections in the close distances (Fig. 12c).

Our triplication study did not find evidence of a broad low velocity zone below the 660-km discontinuity beneath South America and North East Asia because we only study S wave velocity in the two regions. Beneath southern Africa, We studied both P and S wave, although we did not find a broad low velocity zone below the 660-km discontinuity, we find a small P velocity jump and a PREM-like S velocity jump across the 660-km discontinuity, which could be caused by reduced effective bulk modulus in a two-phase zone.

4.3 Depth Distributions of Seismic Anisotropy

Seismic anisotropy and its variation with depth provide important information about composition and crystal alignment in the mantle, with significant implications to the flow and evolution of the mantle. Comparing the seismic observations between SH and SV waves is a direct and powerful way to study the anisotropy along the path of wave propagation. The seismic triplication data recorded in the distance range of 10°–30°, because they sample various depths of the mantle, provide a unique opportunity to probe seismic anisotropy varying with depth (Chen and Brudzinski 2003).

In particular, because various branches have very close ray paths in the shallow mantle (Fig. 5), the upper mantle triplication data recorded for deep events would provide a

unique opportunity for mapping possible anisotropic structures in the bottom of the transition zone and the top of the lower mantle, one of the few regions in the Earth that is reported to be anisotropic.

5 Challenges and Connection to Other Approaches

The major challenges of using the triplication data to constrain seismic structure in the mantle lie in the availability of high-quality dense seismic data and the ability to deal with the effect of lateral variation of seismic structure in the modeling. Dense seismic data now become available through PASSCAL experiments around the world and networks such as the Hi-net in Japan and the US Array in the United States. Dense array data would minimize the effects of the lateral variation of seismic structure. Furthermore, two- or three-dimensional numerical methods, such as the finite-difference technique, can now be employed to study the effects of lateral variation of seismic structure (Song et al. 2004; Song and Helmberger 2006; Wang et al. 2008).

Compared to the studies of the properties of the upper mantle discontinuities using other approaches, such as precursors to the PP and SS phases (Shearer 1991; Shearer and Flanagan 1999; Gu and Dziwonski 2002; Gu et al. 2003; Chambers et al. 2005; Deuss et al. 2006; An et al. 2007) or receiver functions (Niu and Kawakatsu 1996; Shen et al. 1996), the studies using the upper mantle triplication data can constrain the velocity gradients above and below the discontinuity, existence of a low velocity zone and lithospheric lid, P/S velocity ratio, and anisotropy varying with depth, in additional to the velocity jump across the discontinuity and the depth of the discontinuity. These seismic features place significant constraints on mantle temperature, composition and flow. The differential travel time and waveform of the upper mantle triplication are also affected little by the seismic heterogeneities in the shallower part of the mantle, while the precursor studies and receiver function analyses need to deal with the shallower heterogeneities carefully.

Studies using the precursors to the PP and SS phases, however, provide global coverage of the properties of the 660-km discontinuity and the receiver function studies could provide a better lateral resolution in the study region. To better constrain seismic features of the discontinuities, it would be ideal to combine both the waveform modeling of the upper mantle triplicated phases with other approaches, for example, the receiver function analyses. Receiver functions are related to the conversions from the major boundaries in the mantle. They are sensitive to the sharp features of the discontinuities and would be useful for imaging structures of low velocity channels and double discontinuities. In this regard, using the migration method of receiver function (Chen et al. 2005) would be of particular importance in the imaging, as simple stacking of receiver functions is known to produce artifacts such as a “bow-tie” for a deformed discontinuity that can be mistaken as double discontinuities.

6 Conclusions

We review the wave propagation of the triplicated phases and key seismic features that can be studied using the triplicated phases. We discuss the issues for the cases of both shallow and deep events. Triplication data for shallow events can be used to constrain several major features of upper mantle properties: the existence of a lithospheric lid, existence of a low velocity zone beneath a lithospheric lid and P/S velocity ratio varying with depth.

Triplication data for deep events can be used to constrain several key seismic properties near major discontinuities: the velocity gradients above and below the discontinuity, velocity jumps across the discontinuity, and depth extents of different velocity gradients.

We present examples of study for one shallow event sampling the upper mantle beneath southern Africa and two deep events sampling the 660-km discontinuity beneath South America and North East Asia. We also discuss how those key features play an important role in constraining mantle composition and temperature. P and SH triplication data for the shallow event sampling the upper mantle beneath southern Africa suggest presence of a low velocity zone with velocity reductions of at least −5% for S waves and −2% for P waves beneath a 150–210 km thick high-velocity lithospheric lid, and a change of P/S velocity ratio from 1.70 in the lithospheric lid to 1.88 in the transition zone. SH triplication data for the two deep events suggest a similar large velocity gradient extending about 80 km deep below the 660-km discontinuity, but different SH velocity gradients above the 660-km discontinuity and different velocity jumps across the discontinuity beneath the two regions. Beneath South America, the velocity gradient above the 660-km discontinuity is larger than that of PREM, while the velocity jump across the discontinuity is the same as PREM. Beneath northeast Asia, the velocity gradient above the 660-km discontinuity is the same as that of PREM, while the velocity jump across the discontinuity is larger than PREM.

We show that these seismic properties place important constraints on mantle temperature and composition. Beneath southern Africa, the low velocity zone suggests a high temperature gradient of 6°C/km or presence of partial melt. The different P/S velocity ratios between the lithospheric lid and the transition zone suggest a difference in aluminum content of the mantle composition, with values of 1% in the lithospheric lid and 4% in the transition zone, respectively. Beneath southern America and North East Asia, the 80-km depth extent of the larger velocity gradient below the 660-km discontinuity suggests a uniform composition in the lower mantle with an aluminum content of 3.4%. The different velocity gradients above the 660-km discontinuity in two regions suggest either a difference in mantle temperature of about 100°C (with that beneath South America being lower) between the two regions assuming a uniform mantle composition, or alternatively, a difference in aluminum content of about 1.2% (with that beneath South America being lower) between the two regions without invoking a temperature difference between the two regions.

Finally, we discuss the potential of using upper mantle triplication data for further studying some other important features of the mantle: existence of double 660-km discontinuities, existence of low-velocity channels near major discontinuities and anisotropy varying with depth, as well as challenges of the upper mantle triplication study and its connection to other approaches.

Acknowledgments We thank the principal investigators of the Kaapvaal Seismic Array, the BANJO and BLSP for their efforts in collecting the data and the New Chinese Digital Seismic Network (NCDSN) for providing the data, and Sue Webb and Matthew Fouch for the digitized geological boundaries in Africa. This work is supported by an NSF grant #0439978.

References

An Y, Gu YJ, Sacchi M (2007) Imaging mantle discontinuities using least-squares radon transform. J Geophys Res 112. doi:10.1029/2007JB005009

Bercovici D, Karato S (2003) Whole-mantle convection and the transition-zone water filter. Nature 425: 39–44

Brudzinski MR, Chen WP (2000) Variations in P wave speeds and outboard earthquakes: evidence for a petrologic anomaly in the mantle transition zone. J Geophys Res 105:21661–21682
Brudzinski MR, Chen WP (2003) A petrologic anomaly accompanying outboard earthquakes beneath Fiji-Tonga: corresponding evidence from broadband P and S waveforms. J Geophys Res 108. doi:10.1029/2002JB002012
Brudzinski MR, Chen WP, Nowack RL, Huang BS (1997) Variations of P wave speeds in the mantle transition zone beneath the northern Philippine Sea. J Geophys Res 102:11815–11827
Burdick LJ, Helmberger DV (1978) The upper mantle P velocity structure of the Western United States. J Geophys Res 83:1699–1712
Chambers K, Deuss A, Woodhouse JH (2005) Reflectivity of the 410-km discontinuity from PP and SS precursors. J Geophys Res 110. doi:10.1029/2004JB003345
Chen WP, Brudzinski MR (2003) Seismic anisotropy in the mantle transition zone beneath Fiji-Tonga. Geophys Res Lett 30:1682–1696
Chen WP, Tseng TL (2007) Small 660-km seismic discontinuity beneath Tibet implies resting ground for detached lithosphere. J Geophys Res 112. doi:10.1029/2006JB004607
Chen L, Wen L, Zheng T (2005) A wave equation migration method for receiver function imaging: 1.theory. J Geophys Res 110. doi:10.1029/2005JB003665
Cummins PR, Kennett BLN, Bowman JR, Bostock MG (1992) The 520 km discontinuity? Bull Seism Soc Am 82:323–336
Deuss A, Redfern SAT, Chambers K, Woodhouse JH (2006) The nature of the 660-kilometer discontinuity in Earth's mantle from global seismic observations of PP precursors. Science 311:198–201
Dziewonski AM, Anderson DL (1981) Preliminary reference Earth model. Phys Earth Planet Int 25:297–356
Given JW, Helmberger DV (1980) Upper mantle structure of northwestern Eurasia. J Geophys Res 85:7183–7194
Grand SP, Helmberger DV (1984a) Upper mantle shear structure of North America. Geophys J R Astron Soc 76:399–438
Grand SP, Helmberger DV (1984b) Upper mantle shear structure beneath the Northwest Atlantic Ocean. J Geophys Res 89:11465–11475
Gu YJ, Dziwonski AM (2002) Global variability of transition zone thickness. J Geophys Res 107. doi:10.1029/2001JB000489
Gu YJ, Dziwonski AM, Ekstrom G (2003) Simultaneous inversion for mantle shear velocity and topography of transition zone discontinuities. Geophys J Int 154:559–583
Helmberger DV, Wiggins RA (1971) Upper mantle structure of Midwestern United States. J Geophys Res 76:3229–3245
Houard S, Nataf HC (1993) Laterally varying reflector at the top of D'' beneath northern Siberia. Geophys J Int 115:168–182
Jordan TH (1978) Composition and development of the continental tectosphere. Nature 274:544–548
LeFevre LV, Helmberger DV (1989) Upper mantle P velocity structure of the Canadian Shield. J Geophys Res 94:17749–17765
Li L, Weidner DJ (2008) Effect of phase transitions on compressional-wave velocities in the Earth's mantle. Nature 454:984–986
Melbourne T, Helmberger DV (1998) Fine structure of the 410-km discontinuity. J Geophys Res 103:10091–10102
Neele F (1996) Sharp 400-km discontinuity from short-period P reflections. Geophys Res Lett 23:419–422
Niu F, Kawakatsu H (1996) Complex structure of mantle discontinuities at the tip of the subducting slab beneath Northeast China—a preliminary investigation of broadband receiver functions. J Phys Earth 44:701–711
Nyblade AA, Robinson SW (1994) The African superswell. Geophys Res Lett 21:765–768
Obayashi M, Sugioka H, Yoshimitsu J, Fukao Y (2006) High temperature anomalies oceanward of subducting slabs at the 410-km discontinuity. Earth Planet Sci Lett 243:149–158
Shearer PM (1991) Constraints on upper mantle discontinuities from observations of long-period reflected and converted phases. J Geophys Res 96:18147–18182
Shearer PM, Flanagan MP (1999) Seismic velocity and density jumps across the 410- and 660-kilometer discontinuities. Science 285:1545–1548
Shen Y, Solomon SC, Bjarnason IT, Purdy GM (1996) Hot mantle transition zone beneath Iceland and the adjacent Mid-Atlantic Ridge inferred from P-to-S conversions at the 410- and 660-km discontinuities. Geophys Res Lett 23:3527–3530
Simon RE, Wright C, Kgaswane EM, Kwadiba MTO (2002) The P wavespeed structure below and around the Kaapvaal craton to depth of 800 km, from travel times and waveforms of local and regional earthquakes and mining-induced tremors. Geophys J Int 151:132–145

Simon RE, Wright C, Kwadiba MTO, Kgaswane EM (2003) Mantle structure and composition to 800-km depth beneath southern Africa and surrounding oceans from broadband body waves. Lithos 71:353–367

Song TA, Helmberger DV (2006) Low velocity zone atop the transition zone in the western US from S waveform triplication. In: Jacobsen SD, van der Lee S (eds) Earth's deep water cycle. American Geophysical Union, Washington, DC

Song TA, Helmberger DV, Grand SP (2004) Low-velocity zone atop the 410-km seismic discontinuity in the northwestern United States. Nature 427:530–533

Tseng TL, Chen WP (2004) Contrasts in seismic wave speeds and density across the 660-km discontinuity beneath Philippine and the Japan Seas. J Geophys Res 109. doi:10.1029/2003JB002613

Tseng TL, Chen WP (2008) Discordant contrasts of P- and S-wave speeds across the 660-km discontinuity beneath Tibet: a case for hydrous remnant of sub-continental lithosphere. Earth Planet Sci Lett 268:450–462

Walck MC (1984) The P-wave upper mantle structure beneath an active spreading center: the Gulf of California. Geophys J R Astron Soc 76:697–723

Wang Y, Wen L (2007) Geometry and P and S velocity structure of the "Africa anomaly". J Geophys Res 112. doi:10.1029/2006JB004483

Wang Y, Wen L, Weidner DJ, He Y (2006) SH velocity and compositional models near the 660-km discontinuity beneath South America and northeast Asia. J Geophys Res 111. doi:10.1029/2005JB003849

Wang Y, Wen L, Weidner DJ (2008) Upper mantle SH- and P-velocity structures and compositional models beneath southern Africa. Earth Planet Sci Lett 267:596–608

Wiggins RA, Helmberger DV (1973) Upper mantle structure of the Western United States. J Geophys Res 78:1870–1880

Zhang J (1994) Melting experiments on anhydrous peridotite KLB-1 from 5.0 to 22.5 Gpa. J Geophys Res 99:17729–17742

Zhao MC, Langston CA, Nyblade AA, Owens TJ (1999) Upper mantle velocity structure beneath southern Africa from modeling regional seismic data. J Geophys Res 104:47830–47894